Journal of Materials Science & Technology 34 (2018) 355–364

Contents lists available at ScienceDirect

Journal of Materials Science & Technology

journal homepage: www.jmst.org

Vacancy formation enthalpies of high-entropy FeCoCrNi alloy via first-principles calculations and possible implications to its superior radiation tolerance

Weiliang Chen [a,b], Xueyong Ding [a], Yuchao Feng [b], Xiongjun Liu [c], Kui Liu [b], Z.P. Lu [c], Dianzhong Li [b], Yiyi Li [b], C.T. Liu [d], Xing-Qiu Chen [b,*]

[a] School of Metallurgy, Northeastern University, Shenyang 110819, China
[b] Shenyang National Laboratory for Materials Science, Institute of Metal Research, Chinese Academy of Sciences, Shenyang 110016, China
[c] State Key Laboratory for Advanced Metals and Materials, University of Science and Technology Beijing, Beijing 100083, China
[d] Center of Advanced Structural Materials, Department of Mechanical and Biomedical Engineering, College of Science and Engineering, City University of Hong Kong, Kowloon, Hong Kong, China

ARTICLE INFO

Article history:
Received 1 August 2017
Received in revised form
22 September 2017
Accepted 25 October 2017
Available online 2 November 2017

Keywords:
FeCoCrNi
Point defects
Vacancy formation enthalpy
First-principles calculations
Modeling high-entropy alloys

ABSTRACT

Because atoms in high-entropy alloys (HEAs) coordinate in very different and distorted local environments in the lattice sites, even for the same type of constituent, their point defects could highly vary. Therefore, theoretical determination of the thermodynamic quantities (i.e., defect formation enthalpies) of various point defects is rather challenging because each corresponding thermodynamic quantity of all involve constituents is not unique. The knowledge of these thermodynamic quantities is prerequisite for designing novel HEAs and understanding the mechanical and physical behaviors of HEAs. However, to date there has not been a good method to theoretically derive the defect formation enthalpies of HEAs. Here, using first-principles calculations within the density functional theory (DFT) in combination of special quasi-random structure models (SQSs), we have developed a general method to derive corresponding formation enthalpies of point defects in HEAs, using vacancy formation enthalpies of a four-component equiatomic fcc-type FeCoCrNi HEA as prototypical and benchmark examples. In difference from traditional ordered alloys, the vacancy formation enthalpies of FeCoCrNi HEA vary in a highly wide range from 0.72 to 2.89 eV for Fe, 0.88–2.90 eV for Co, 0.78–3.09 eV for Cr, and 0.91–2.95 eV for Ni due to high-level site-to-site lattice distortions and compositional complexities. On average, the vacancy formation enthalpies of 1.58 eV for Fe, 1.61 eV for Cr, 1.70 eV for Co and 1.89 eV for Ni are all larger than that (1.41 eV) of pure fcc nickel. This fact implies that the vacancies are much more difficult to be created than in nickel, indicating a reasonable agreement with the recent experimental observation that FeCoCrNi exhibits two orders of amplitudes enhancement of radiation tolerance with the suppression of void formation at elevated temperatures than in pure nickel.

1. Introduction

Vacancies in alloys are unavoidable, and their concentration increases with the temperature [1,2]. Thermodynamically, the enthalpy of vacancy formation in alloys defines the requested energy to create a single vacancy at the lattice sites, and its value is related to the thermodynamics and kinetics of vacancy defects, such as vacancy-as-media activation energy barrier of diffusion, nucleation energy of precipitations, impurity solubility and local segregates, microsegregation, creeps and corrosion and so on. Experimentally, vacancy formation energy can be determined by traditional experimental methods, such as positron annihilation spectroscopy [3] and differential dilatometry [4]. Usually, experimentally measured vacancy concentration c_v to the temperature T is linearly fitted to the Arrhenius law using the thermodynamic relation, $G_f = H_{0K} - TS_f$ (G_f-Gibbs energy of vacancy formation, H_{0K}-the vacancy formation enthalpy extrapolated at $T = 0$ K and S_f - the entropy). Thus, the vacancy formation enthalpy can then be derived by the slop of the $\ln c_v$ versus $1/T$ plot. Nowadays, first-principles calculations have been widely used to derive the vacancy forma-

* Corresponding author.
E-mail address: xingqiu.chen@imr.ac.cn (X.-Q. Chen).

https://doi.org/10.1016/j.jmst.2017.11.005
1005-0302/

tion enthalpy [1,2,5–10] in an acceptable accuracy. However, most of computational methods dealing with vacancies apply to various materials with ordered lattices.

Recently, a revolutionary alloy design strategy, i.e., the entropy stabilization concept, was proposed in the metal community, and interesting properties are continuously found in these so-called high-entropy alloys (HEAs) whose constituents have an equiatomic or nearly equiatomic ratio [11–52]. Due to the maximization of the configuration entropy, this new family of alloys show unique features and outstanding properties including ultrahigh low-temperature toughness, ultrastable phase stability and high strength at elevated temperatures, and prominent irradiation resistance [43,44]. In these highly concentrated alloys, lattices are severely distorted and conventional concepts of "solutes" and "solvents" lose their original meaning. In other words, knowledge regarding the atomic site occupation in HEAs, which is inevitably associated with vacancy formation tendency, remains mysterious, leading to difficulties in fully understanding their unique properties and deformation behaviors. For example, HEAs have shown a significant enhancement of ion radiation tolerance by two orders of magnitude with the suppression of void formation at elevated temperatures due to their high-level site-to-site lattice distortions and compositional complexities, making them extremely promising for irradiation tolerant applications [43,44,60]. Previous studies indicate that defect dynamics including defect generation, interaction and migration are critical to fully understand the fundamental controlling mechanism on an enhanced radiation tolerance. Therefore, knowledge and information regarding vacancy formation and interstitial-vacancy recombination are indispensable for this purpose.

However, the theoretical calculations of defects thermodynamics are difficult for the type of HEAs. Within the currently available theoretical technologies and the framework of the density functional theory, it is hard to simulate HEAs in reality being the same as real HEAs because the periodic unit cells are limited in the number of lattice sites but the possibilities of the random atomic distributions in HEAs are too many to be completely sampled. As performed in many previous calculations [53–67], a compromise strategy is to adopt the random solid solution model of special quasi-random structures (SQSs) [68]. It is well known that SQSs were designed for small-unit-cell periodic structures that closely mimic the most relevant near neighbor pairs and multisite correlation functions of random substitutional alloys. To predict the single-phase HEAs, one of the recent progresses was the proposed effective *ab initio* modeling [61] using a set of small ordered SQS structures, whose weight-averaged properties approximate those of the truly random alloys, and another progress was to seek specific combinations of elements most likely to form single-phase HEAs [64] through the use of high-throughput computation of the enthalpies of formation of a series of binary compounds. Given the fact that the underlying chemical complexity of multi-component solution alloys exhibits a wide range of the formation and migration energies of vacancies and interstitials, the so-called method has been suggested by accounting first-nearest neighboring atoms to classify the type of defects using ab initio calculations and SQSs with an aim of deriving the distribution of defect formation energies and migration barriers in four Ni-based solid-solution alloys [66]. Furthermore, To simulate electronic, magnetic and transport properties of single-phase HEAs, several nice attempts have been done using the KKR-CPA method which considers the effects of chemical disorder on the electronic states, and delivers the configurationally averaged properties [60] and using the Monte Carlo method and magnetic cluster expansion (MCE) which has been successfully applied to describe a broad range of magnetic and structural transformation effects in magnetic solid-solution alloys to study short-range order, atomic displacements, electronic density of states, and magnetic moments [57,69,70]. Although great progresses have been made [53–70], the more difficult task is the theoretical determination of various thermodynamics of defects (i.e., vacancy) for HEAs due to high-level site-to-site lattice distortions and compositional complexities. Following the spirit to consider all possible relevant small-unit-cell periodic structures by combining SQSs and first-principles calculations, here we propose a general method to reasonably derive the vacancy formation enthalpies for HEAs. As a specified case, we selected a four-component equiatomic HEA alloy of FeCoCrNi which has a single fcc structure [11,12] based on experimental observations. In addition, this FeCoCrNi HEA was recently revealed to exhibit almost two orders magnitudes enhancement of radiation tolerance with the suppression of void formation than in pure nickel at elevated temperatures [43,44]. Therefore, it also urges to understand the underlying mechanism for the enhanced radiation tolerance of HEAs.

2. Modeling

Assuming a n-component equiatomic HEA, we seek all possible small-unit-cell periodic structures within the SQS framework. For each ordered structure, through first-principles calculations, the vacancy formation of enthalpy, H_v, can be derived as

$$H^i_{SQS}\left(X^j_{Vac}\right) = E^i_{SQS}\left(X^j_{Vac}\right) - E^i_{SQS} + E^{Solid}_X \quad (1)$$

where $E^i_{SQS}\left(X^j_{Vac}\right)$ is the calculated total energy of the i-th-occupation SQS with a single X-atom vacancy, E^i_{SQS} the total energy of the i-th-occupation SQS without any vacancy, E^{Solid}_X the total energy of X-atom at its ground-state solid phase, and $H^i_{SQS}\left(X^j_{Vac}\right)$ the derived vacancy formation enthalpy of the i-th-occupation equiatomic SQS with a single X-atom vacancy. For a given n-component HEA with equiatomic ratios occupying the m-atom ordered SQS structure, the i parameter should have a maximum value, and $i = A^{n-1}_n$ and the j parameters can be taken in the range from 1 to m/n. For instance, for a four-component equiatomic HEA, i ranges from 1 to 24 and j ranges from 1 to 5 (each j denotes a different position occupied by X atom in the SQS structure), if the atomic number of the SQS is fixed to be 20. Within this consideration, E^i_{SQS} with and without X-atom vacancy needs to be optimized through first-principles calculations.

It is reasonable to see that all these i-th-occupation SQS structures indeed consider all possible relevant near neighbor pairs and multisite correlation functions of random substitutional HEAs within the given and same SQS structure. Theoretically, their possibilities to occur within the small-unit-cell ordered SQS structure should be the same. Therefore, this provides a fundamental basis for the statistical average. With $H^i_{SQS}\left(X^j_{Vac}\right)$ for i-th-occupation SQS with j-th vacancy for the X-atom, the vacancy formation enthalpy in the statistical way for HEA is derived as

$$H^{Vac}_X = \left[\sum_{i=1}^{A^{n-1}_n}\sum_{j=1}^{m/n} H^i_{SQS}(X^j_{Vac})\right] \Big/ \left(\frac{mA^{n-1}_n}{n}\right) \quad (2)$$

It needs to be emphasized that, within such a framework, the computationally time-consuming costs are huge. With increasing the number of components and atomic sites in HEAs, the possible occupational configurations increase exponentially. Therefore, the control of the proper size for the selected small-unit-cell SQS structure should be compromised but reasonable as small as possible, so that the computational efforts can be reasonably reduced to meet our currently available supercomputer resources.

Table 1
DFT-obtained lattice parameters, equilibrium volumes, and enthalpies of formation for 24-ocupation configuration of the 20-atom-unit-cell ordered SQS structure.

i-th configuration	α (Å)	b (Å)	c (Å)	α (°)	β (°)	γ (°)	V (Å3/uc)	$\triangle H$ (meV/atom)
1 CrFeCoNi	8.60	4.29	9.03	56.04	104.36	70.79	217.64	84.5
2 CrFeNiCo	8.66	4.33	9.00	56.06	103.66	70.16	220.51	78.8
3 CrCoFeNi	8.59	4.27	8.95	56.20	104.20	70.74	215.89	102.0
4 CrCoNiFe	8.56	4.29	8.94	55.68	103.67	70.74	215.35	100.8
5 CrNiFeCo	8.67	4.32	9.01	56.23	103.95	70.60	222.08	71.2
6 CrNiCoFe	8.55	4.29	8.92	55.80	103.60	71.03	216.40	105.3
7 FeCrCoNi	8.58	4.28	8.95	56.02	104.09	70.59	214.98	87.4
8 FeCrNiCo	8.60	4.27	8.96	55.96	104.14	70.93	216.21	90.2
9 FeCoCrNi	8.57	4.28	8.93	56.02	103.82	70.62	215.14	88.6
10 FeCoNiCr	8.56	4.29	8.93	55.89	103.80	70.65	214.95	100.5
11 FeNiCrCo	8.57	4.27	8.93	55.84	103.82	70.84	214.84	101.2
12 FeNiCoCr	8.63	4.32	9.05	56.03	103.99	70.74	221.60	73.1
13 CoCrFeNi	8.61	4.31	9.02	55.95	104.04	71.00	220.42	65.0
14 CoCrNiFe	8.59	4.28	8.97	55.90	104.08	71.39	217.96	59.4
15 CoFeCrNi	8.58	4.29	8.94	55.99	103.72	70.83	217.37	78.7
16 CoFeNiCr	8.57	4.28	8.96	55.83	104.02	71.02	215.69	96.7
17 CoNiCrFe	8.58	4.29	8.99	55.81	104.00	71.10	218.08	77.3
18 CoNiFeCr	8.60	4.30	9.01	56.04	104.20	70.53	217.39	93.0
19 NiCrFeCo	8.56	4.27	8.95	55.89	104.04	71.07	215.59	71.2
20 NiCrCoFe	8.57	4.28	8.98	55.73	103.95	71.26	217.13	90.5
21 NiFeCrCo	8.62	4.32	9.05	55.72	103.90	71.86	224.81	63.9
22 NiFeCoCr	8.64	4.30	9.03	56.13	104.12	70.69	219.96	80.6
23 NiCoCrFe	8.67	4.32	9.01	55.90	103.89	70.71	221.21	70.9
24 NiCoFeCr	8.60	4.29	9.00	56.18	104.54	70.91	217.66	93.8

3. Computational details

3.1. First-principles calculations

All the energies are computed within the Vienna *Ab Initio* Simulation Package (VASP) [71,72] with the projector augmented wave (PAW) method [73,74] and generalized gradient approximation Perdew-Burke-Ernzerhof functional (GGA-PBE) [75]. The cutoff energy of the plane waves is 350 eV and Brillouin zone integration is performed by the Monkhorst-Pack scheme with a $5 \times 5 \times 5$ *k*-point meshes. It needs to be emphasized that those 24 ordered SQSs structures are fully relaxed, but the vacancy formation enthalpies are calculated at a fixed volume and a fixed shape of 480 supercells and, in the meanwhile, all atoms in supercells have to be allowed to be fully relaxed. The positions of the atoms in the supercells are relaxed with tolerances of 0.01 eV/Å for the atomic force and 1×10^{-5} eV/atom for the total energy. Spin-polarized calculations were performed by assuming same spin directions before optimizations. Once the Hellmann–Feynman force acting on atoms is less than 0.01 eV/Å, the atoms are regarded as being fully relaxed. After the optimizations, the spin configurations vary.

3.2. Small-unit-cell ordered SQS structure

In order to construct a suitable small-unit-cell periodic supercell for the FeCoCrNi HEA, we employed the tool of the Alloy Theoretic Automatic Toolkit (ATAT) [76] within the framework of special SQS degenerated by the so-called mcsqs algorithm [77]. Here, to comply with our currently available computational resources, the compromise has to be adopted by suitably constructing a 20-atom ordered SQS supercell with the fcc structure. The mcsqs method is based on a Monte Carlo simulated annealing loop with an objective function that seeks to perfectly match the maximum number of correlation functions and optimizes the shape of the supercell jointly with the occupation of atomic sites. With the mcsqs method, it ensures that the obtained configuration space is exhaustive and unbiased by a pre-specified supercell shape.

3.3. Occupational configurations of ordered SQS structures and the configuration supercells including vacancy

On basis of constructed 20-atom ordered SQS structure for the FeCoCrNi HEA, in total we have 24 different occupational configurations according to $i = A_4^3$. However, in order to calculate the vacancy formation enthalpy, we have to consider all possible vacancies even for the same type *X* atom, because in this ordered SQS structure each *X* atom indeed has different neighboring local coordinators. Theoretically, within the SQS supercell there are 5 different positions of the single vacancy even for the same *X* atom. Statistically, we need to perform calculations of 480 supercells including the monovacancy (here, we select $2 \times 1 \times 1$ supercell of SQS structure) and optimize the atomic sites by minimizing the interatomic force. Noted that during these calculations the volume and shape of monovacancy-containing supercells were not allowed to be relaxed in order to further reduce the time-consuming costs but all atoms have to be relaxed. In other words, for each *X* component (*X* = Fe, Co, Cr, Ni), we need to perform the calculations of 120 supercells by considering all possible occupations in 24 different occupational configurations.

4. Results and discussion

4.1. SQS structures and enthalpy of formation

According to 20-atom ordered SQS structures of the FeCrCoNi HEA, we have performed the optimizations by considering all possible configurations of occupations. The obtained lattice parameters, equilibrium volumes, and derived enthalpies of formation are now summarized in Table 1. It can be seen that the structural distortions by varying different configurations highly differ. For each configuration, we have derived its enthalpy of formation as plot in Fig. 1. It can be seen that upon different occupation configurations, the enthalpy of formation is obviously scattering from the lowest 59.4 meV/atom to the highest 105.3 meV/atom. However, the average value of the enthalpy of formation is 84.4 meV/atom, in nice agreement with the previously calculated data of 77 meV/atom which was obtained using the larger 24-atom SQS structure [58]. The convergence test demonstrated that even in the small cell the

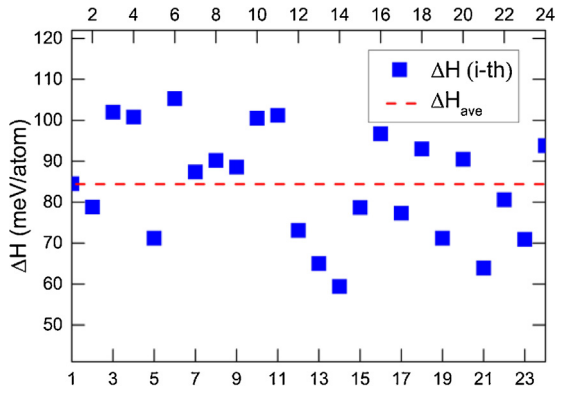

Fig. 1. DFT-derived enthalpies of formation (ΔH, meV/atom) for 24 occupation configurations of the ordered SQS structure.

derived enthalpy of formation in average is relatively reasonable, albeit with a bit more scatter. Occasionally, one of structures, No. 1 configuration, has an enthalpy of formation of 84.5 meV/atom that is very close to the averaged value.

It needs to be noted that, because the calculated enthalpies of formation are all positive, demonstrating that all considered structures of HEAs are thermodynamically metastable at the ground state of absolute zero Kelvin and they should be metastable at a certain temperature, in agreement with the random substitutional distribution in the fcc structure. If we consider the contribution of configuration entropy to the total free energy ($G = H_{HEA}$-$TS_{conf.}$; here H_{HEA} = 84 meV/atom from our current calculated value and the configuration entropy of $S_{conf.} = 1.386R = 0.1196$ meV/K per atom for four-component FeCoCrNi directly taken from Ref. [12,57]) and, meanwhile, the vibrational entropy (corresponding to atomic vibrations) is ignored, the upper bound temperature of stabilizing FeCoCrNi HEA (namely, $G < 0$) can be estimated to be 750 K. If the vibrational entropy is be further contained, the corresponding temperature to make $G < 0$ will be significantly reduced. This fact provides the robust evidence that the FeCoCrNi HEA is a typically entropy stabilized alloy. In our current calculations, we did not calculate the vibrational entropy, which, in principles, can be also calculated according the constructed 24 SQS structures using much more supercomputer resources. This will be reported in the forthcoming paper.

Additionally, the previous study ever suggested the concept of the mixing enthalpy ΔH_{mix} of a multi-component alloy as

$$\Delta H_{mix} = \sum_{i=1, j\neq 1}^{n} c_i c_j \omega_{ij} \quad (3)$$

where c_i is the atomic percent of the i-th component, n the number of the alloy component, and $\omega_{ij} = 4\Delta H_{ij}$ with ΔH_{ij} being the mixing enthalpy for equiatomic binary alloys calculated through the empirical macroscopic Miediema's model [78,79] and the first-principles density functional theory (DFT) calculations [64]. For FeCoCrNi HEAs, there are six equiatomic binary compounds (FeCo, FeCr, FeNi, CoCr, CoNi and CrNi). Their mixing enthalpies are listed in Table 2. From Table 2, according to Eq. (3) using the inputs of the equiatomic binary mixing enthalpies the derived mixing enthalpies of FeCoCrNi are both negative, −52.8 meV/f.u. and −56.5 meV/f.u., respectively. In comparison with our currently DFT calculations using the 24 configurations of the ordered SQS structure in average, the discrepancies are very large. This fact reveals that the traditional and simple concept of the mixing enthalpy using Eq. (3) has much space to be improved. The main reason for this can be attributed to the fact that Eq. (3) only expresses a simple numerical mixing which is lacking of physical insights.

Table 2
Mixing enthalpies of six equiatomic binary alloys derived through the first-principles high-throughput DFT calculations and by the empirical Miedema's macroscopic models. The derived mixing enthalpy via Eq. (3) is also in comparison with our currently DFT calculations using the 24 configurations of the ordered SQS structure in average. The unit of the mixing enthalpy is meV/atom. Noted that the ΔH values obtained by Miedema's macroscopic models and by experiments are taken from the Ref. [78,79] and the DFT values are from the Ref. [64] for all six binary compounds.

Mixing enthalpy (meV/atom)	FeCo	FeCr	FeNi	CoCr	CoNi	CrNi	FeCoNiCr
ΔH [DFT]	−8	−60	−97	5	−30	−21	−52.8
ΔH [Mie]	−10	−20	−20	−72.5	0	−103	−56.5
ΔH [Exp]	−103	61	−40	27	6	66	4.3
ΔH [This work; DFT values of the 24 configurations in average]							84.4
ΔH (SQS [57])							76.7
ΔH (SRO [57])							15.8

4.2. Vacancy formation enthalpy

Usually, vacancies are formed by removing an atom from its regular and ordered lattice positions in ordered structures. However, although vacancies are defined as what we adopt in ordered structures, in HEAs the neighboring atoms in each lattice sites are different. This is mainly because of their random substitutional distributions and distorted local environments. The difference in the local atomic configuration certainly results in different interatomic interactions, thereby having different energies for each site even for the same type atoms in HEAs. This fact means that their vacancies for the same X-type atom can be different, suggesting that their vacancy formation enthalpies should be in a spectrum of values. With the optimized 24 ordered SQS structures considering all possible occupations of the FeCrCoNi HEA, we first constructed $2 \times 1 \times 1$ supercells. Within this framework, we considered all possible vacancies and therefore we have performed 20 different optimizations by creating the single vacancy for each atom in a given supercell. This means that each type of atoms in a supercell will have five different single vacancies. In total, we will obtain 120 values of the vacancy formation enthalpy for the same X-type atom from 24 different supercells.

Fig. 2 complies the vacancy formation enthalpies of each Fe, Cr, Co and Ni atom in the FeCrCoNi HEA. The common feature for Fe, Cr, Co and Ni is that their vacancy formation enthalpies highly vary. As shown in Fig. 2, the Fe vacancy formation enthalpy varies from the lowest 0.72 eV to the highest 2.89 eV. It is mainly because the different neighboring coordinators in the vicinity around the targeted

Table 3
Vacancy formation enthalpies (averaged H_X^{Vac} and H_{SQS}^{i} in eV) at 0 K of the FeCrCoNi HEA in comparison to those of the ordered fcc-type Fe, Cr, Co and Ni metals.

	H_X^{Vac} (Calc.)	Distribution of H_{SQS}^{i} (Calc. in%)				Fcc (Calc.)	Fcc (Expt.)
	eV	<1.0	1.0–1.5	1.5–2.0	>2.0	eV	eV
Fe	1.58	12.5	28.3	39.1	20.0	1.89 (this work), 1.86 [9]	
Cr	1.61	9.1	35.8	35.8	20.8	1.62 (this work), 1.58 [9]	
Co	1.70	3.3	36.7	36.7	23.3	1.85 this work), 1.83 [9]	
Ni	1.89	2.5	49.1	49.1	34.2	1.41 (this work), 1.46 [9]	1.79 [80] 1.45–1.80 [80]

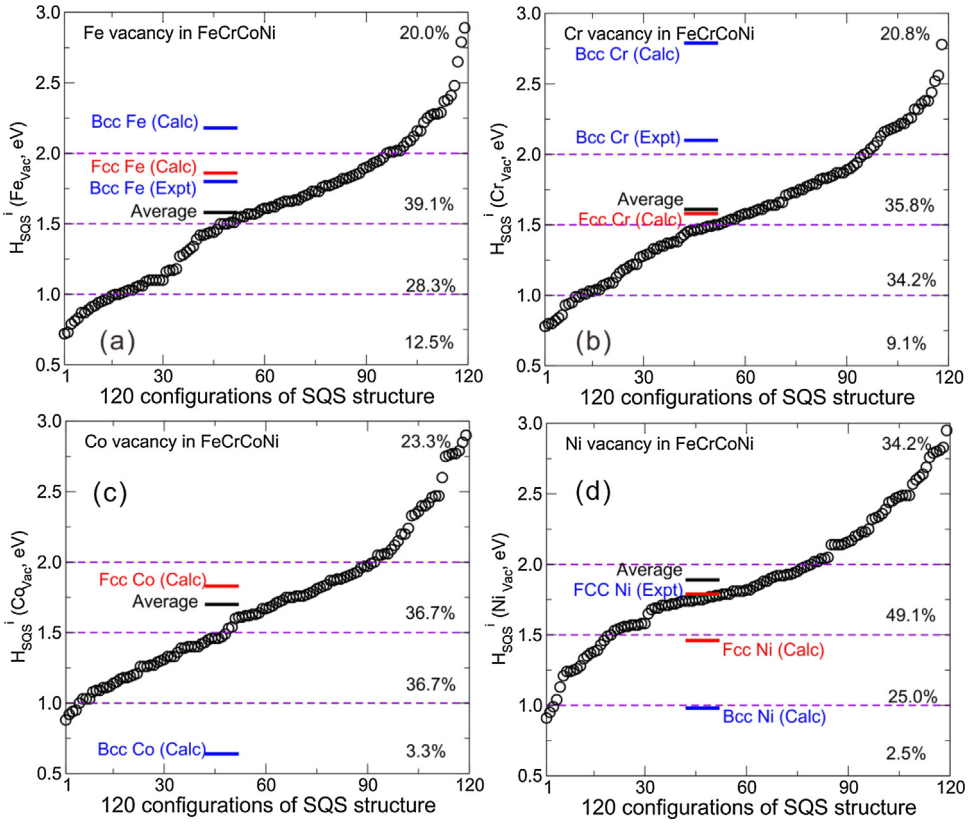

Fig. 2. Vacancy formation enthalpies (in eV) for each type of atoms in FeCrCoNi HEAs. Note that for each type of atom we have 120 different calculations by all possible local configurations. These data are compiled in an ascending order. In comparison, we also list the vacancy formation enthalpy of each type *X* atom in its solid and ordered fcc and bcc structures.

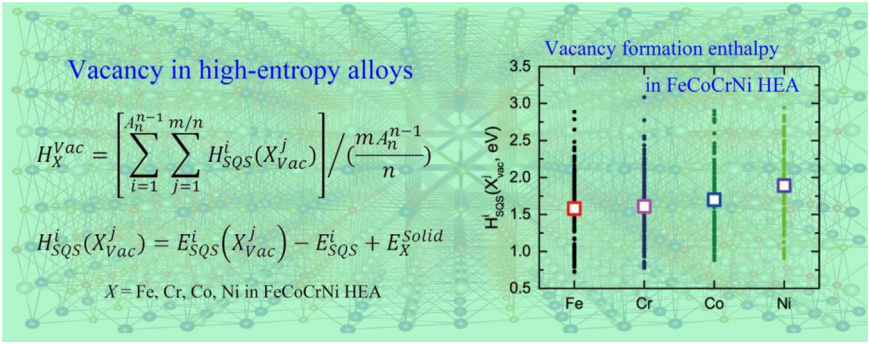

Fig. 3. Average vacancy formation enthalpies (in eV) for each type of atoms in FeCrCoNi HEAs.

vacancy. For instance, the Fe vacancy with the lowest enthalpy of vacancy formation of 0.72 eV has five Fe, five Cr and two Ni atoms in its first nearest-neighbor shell and, however, the Fe vacancy with the highest formation enthalpy (2.89 eV) only has one Fe, two Cr, and two Co as well as seven Ni atoms. The statistic distributions demonstrate that, among 120 different values, 12.5% with a value below 1.0 eV, 28.3% from 1.0 eV to 1.5 eV, 39.1% from 1.5 eV to 2.0 eV, and 20% above 2.0 eV. The Cr vacancy formation enthalpy changes from 0.78 eV to 3.09 eV among which the data below 1.0 eV occupy 9.1%, between 1.0 eV and 1.5 eV have a weight of 34.2%, from 1.5 eV to 2.0 with a weight of 35.8, above 2.0 eV show a weight of 20.8%. However, for both Co and Ni vacancy formation enthalpies the data below 1.0 eV are 3.3% and 2.5%, respectively, which are less than those of Fe (12.5%) and Cr (9.1%). The data in the range above 1.5 eV in both Co and Ni are apparently more than those of both Fe and Cr. These results imply that, in the viewpoint of the statistics, the vacancies of both Ni and Co should be more difficult to be created than both Fe and Cr in the FeCrCoNi HEA.

Furthermore, according to Eq. (2) we have also derived the average enthalpy of vacancy formation for Fe, Cr, Co and Ni atoms in the FeCrCoNi HEA. As illustrated in Table 3, it can be seen that the average enthalpy of Ni has the highest value of 1.89 eV for a vacancy per Ni and the Fe and Cr have almost the same average enthalpy of vacancy formation, 1.58 eV and 1.61 eV, respectively. The Co vacancy formation enthalpy is 1.70 eV in between Ni and Fe (Cr). These values have been further compiled in Fig. 3. Because the FeCrCoNi HEA crystallizes in the fcc structure, it will be meaningful that we compare their average enthalpies of vacancy formation

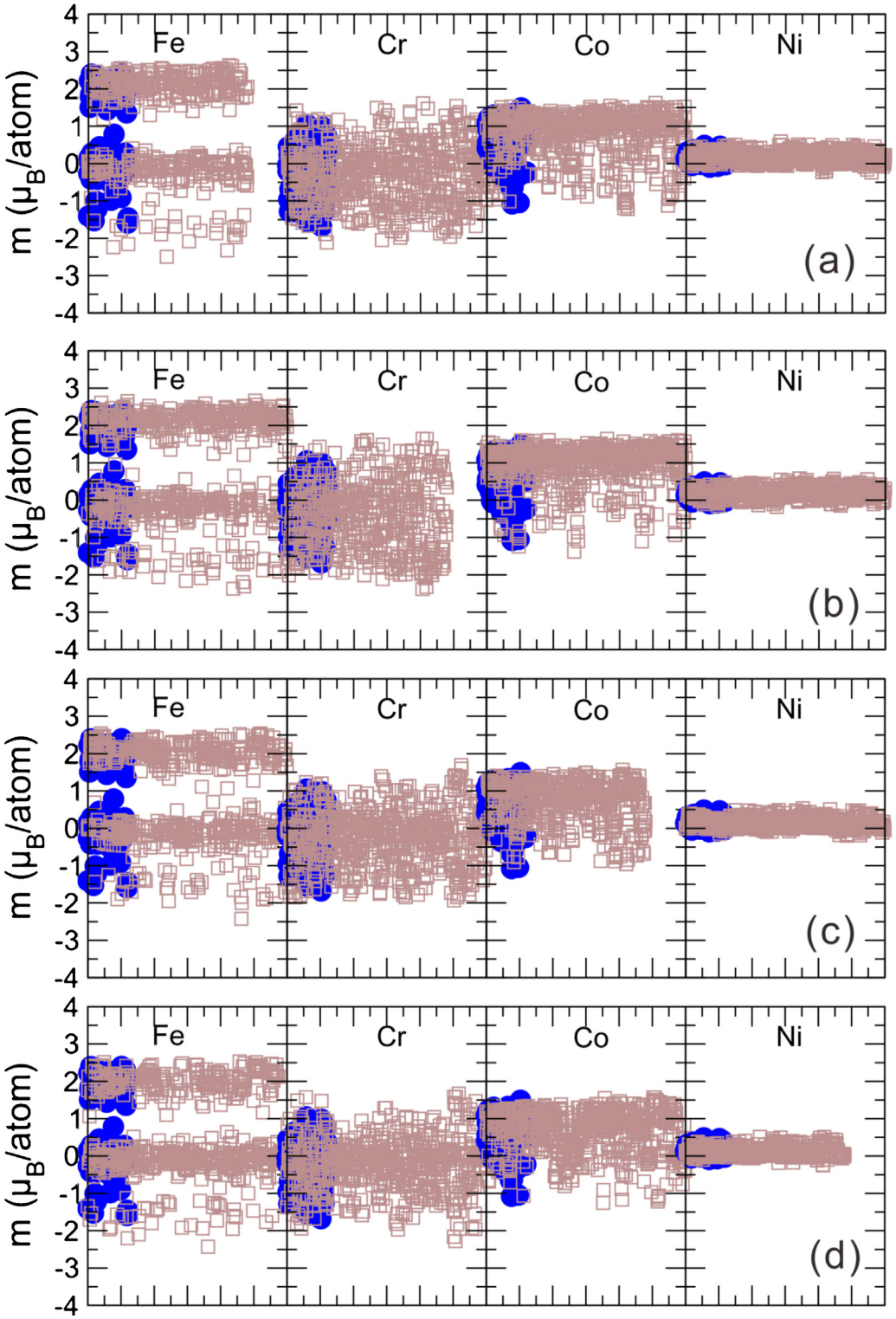

Fig. 4. Influence of the vacancy on the local magnetic moments in the FeCrCoNi HEA. In panel (a) the Fe-, Cr-, Co- and Ni-magnetic moments with the presence of a Fe single vacancy; Panel (b), the Fe-, Cr-, Co- and Ni-magnetic moments with the presence of a Cr single vacancy; Panel (c) the Fe-, Cr-, Co- and Ni-magnetic moments with the presence of a Co single vacancy; Panel (d) the Fe-, Cr-, Co- and Ni-magnetic moments with the presence of a Ni single vacancy. Note that all magnetic moments (hollow squares) with the presence of the vacancy are compared with the magnetic moment (solid circles) without any vacancies.

with the DFT-derived values of their constituents in their specified ground-state fcc phases in Table 3. The results show that the formation enthalpies of Fe and Co vacancies in FeCrCoNi are lowered by 0.31 eV and 0.15 eV than those of pure fcc Fe and Co, respectively. However, both Cr and Ni show a different tendency. The averaged value of Cr (1.61 eV) is almost identical to that of the pure fcc Cr (1.62 eV), but the averaged value of the Ni vacancy (1.89 eV) in FeCrCoNi is higher than that of fcc Ni (1.41 eV).

It needs to be emphasized that in the previous work [67] the vacancy formation enthalpies in the FeCrCoNi HEA was calculated

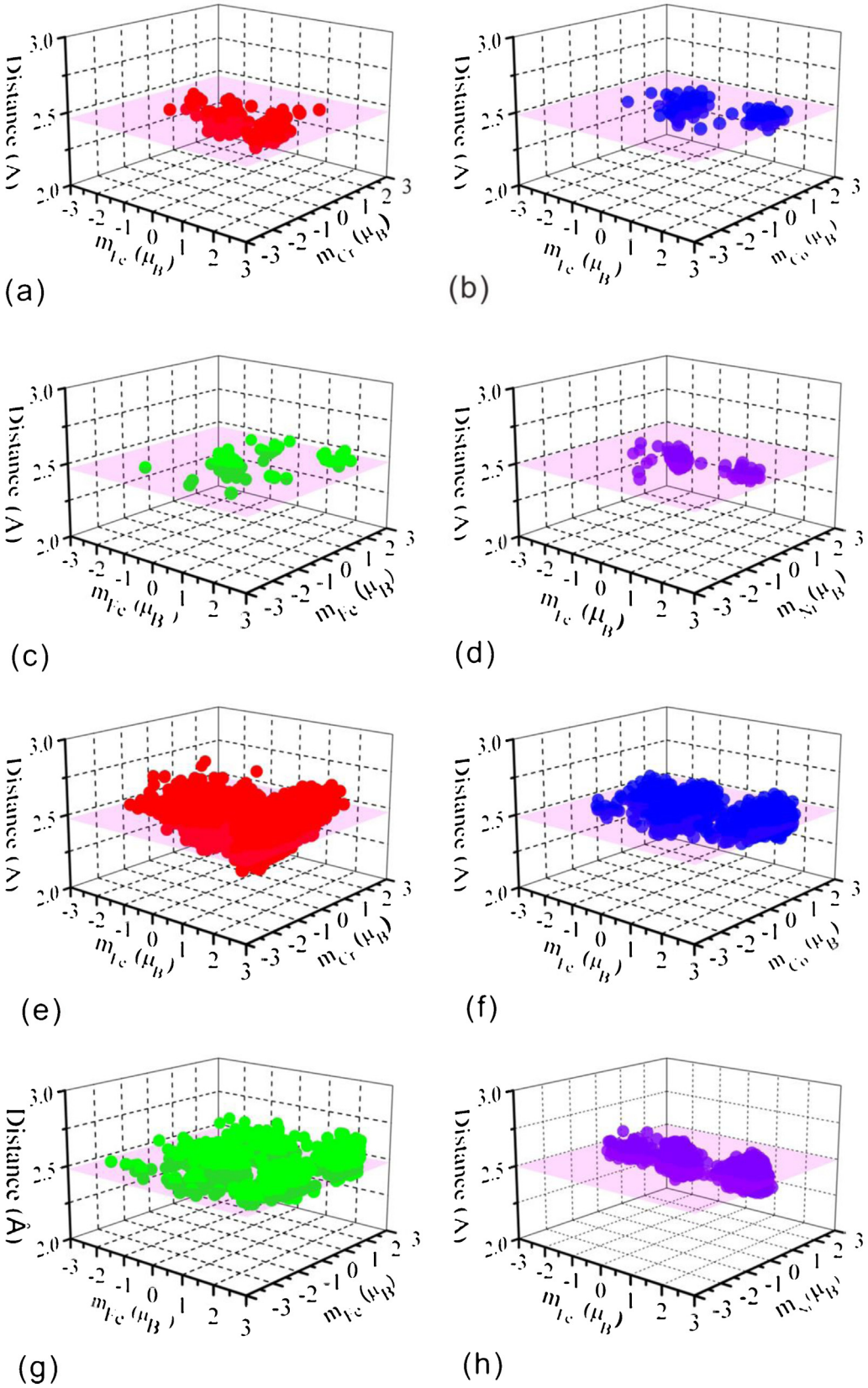

Fig. 5. 3D visualization of the nearest neighboring distances and their local moments of Fe-Cr (a), Fe-Co (b), Fe-Fe (c) and Fe-Ni (d) for the FeCrCoNi HEA without any vacancies; Panels (e, f, g, and h) are the 3D visualized nearest neighboring distances related with their local moments of Fe-Cr (e), Fe-Co (f), Fe-Fe (g) and Fe-Ni (h) for the FeCrCoNi HEA with a Fe single vacancy. The red plane denotes the averaged nearest neighboring distance.

by using twenty different classes configurations of 32-atom SQS cell. But, they did not consider different occupational configurations [67]. In comparison with the previous calculations [67], the vacancy formation enthalpies of Fe, Co and Ni are positive also with a range from 1.5 eV to 3.0 eV for Fe, from 1.2 eV to 2.0 eV for Co, and from 1.5 eV to 2.6 eV for Ni. This tendency is roughly consistent with our current calculations. However, the differences are two aspects. Firstly, in Ref. [67], the average vacancy formation enthalpy of Fe was revealed to be the highest among all these four constituents and it is even higher than that of pure fcc Fe. However, in our work the average vacancy formation enthalpy of Fe is lower than that of pure fcc Fe. We further discovered that the highest average vacancy formation enthalpy is Ni. Secondly, the total difference is that in Ref. [67] Middleburgh et al. reported that most of Cr monovacancy in FeCrCoNi HEA carries negative vacancy formation enthalpy with two monovacancy site of Cr showing the positive enthalpy. These results were substantially different from our current calculations in which our obtained vacancy formation enthalpy for each Cr site exhibits the positive value among the 480 calculations of 120 configurations of our current modeling. Physically, as a typical defect of vacancy, the positive enthalpy is apparently reasonable otherwise any defect with negative enthalpies will simultaneously and naturally occur. In addition, because no any structural information was given in Ref. [67], we cannot reproduce their results.

Recently, experiments [43,44] revealed that, under the same irradiation damage level with 1.5 MeV Ni^+ ions to 3×10^{15} cm^{-2} at 773 K, the FeCrCoNi HEA exhibits a much higher swelling resistance than in pure Ni. Specifically, nickel shows a significant overall swelling of about 1.8% but the FeCrCoNi HEA exhibits substantially lower void swelling with a value of as low as about 0.02%, more than two orders of magnitude lower than in nickel. It should be emphasized that in the early stages of irradiation the vacancy formation is important to understand the irradiation-resistant ability. The larger average vacancy formation enthalpies of Fe (1.58 eV), Co (1.61 eV), Cr (1.70 eV) and Ni (1.89 eV) in the FeCoCrNi HEA than that (1.41 eV) of pure nickel imply that the creation of vacancies is more difficult in HEA than in pure nickel. In particular, it needs to be emphasized that the average vacancy formation enthalpy is 1.89 eV for Ni in FeCoCrNi, which is much larger by 34% than that of pure nickel. These facts seem interpret well the experimental observation that the FeCoCrNi HEA shows a better irradiation-resistant ability in the early stage of ion irradiation. Of course, it also needs to be emphasized that the irradiation-resist behavior of materials is highly complex, depending on various factors, such as migration barriers, interstitial-vacancy recombination, and cluster formation, etc. In our current work, all these factors have not been computed. In addition, it needs to be addressed that in general the threshold value (a few ten eV, commonly assumed as 40 eV) of atomic displacements under irradiation is much higher than those so-called enthalpies of vacancy formation. Therefore, here we only address that the vacancy formation refers to the early stage of irradiations. It should be noted that at the early stage of irradiations the lowest enthalpy of vacancy formation may be directly related with the irradiation-resistant behavior. However, in our current case of FeCoCrNi HEA the weights of the lowest enthalpies of vacancy formation are very low for all four types of monovacancies (see Fig. 2).

4.3. Local magnetic moments

Furthermore, in order to see the influence of the vacancy on the magnetic moments of each type of atoms in the FeCrCoNi HEA, we have plotted the local moment distributions with and without vacancy for all considered 24 ordered structures and 120 vacancy-contained structures in Fig. 4. As expected, vacancy shows some certain influences on the local magnetic moments. From Fig. 4, in all cases three types of local moments can be observed for Fe atoms, most around positive 2.0 μ_B/atom and $\pm 0.1 - \pm 0.3$ μ_B/atom, but a few Fe atoms with about -1.2 μ_B/atom. Note that the positive spin moment of magnetism denotes the spin direction to be the same as that in the initial ferromagnetic orderings, whereas the negative spin moment corresponds to their opposite spin directions to those ferromagnetic orderings. The Cr atoms carry the local spin moment in a wide range from -2.0 μ_B/atom to 1.0 μ_B/atom but over 80% Cr atoms have negative local moments. In contrast, both Co and Ni atoms show less scattered local moments with respect to both Fe and Cr. The Co atom typically carries the positive local moments about 1.0 μ_B/atom and the local moment is typically about 0.4 μ_B/atom for all Ni atoms.

In addition, it needs to point out that for the case without any vacancy this trend of local magnetic moment is nice agreement with the previously calculated data obtained using the larger 108-atom SQS structure without any vacancy [57]. Certainly, some discrepancies of their absolute local magnetic moments definitely exist and the reason can be attributed to the size of structural models or the quantity of statistical samples. In Ref. [57] only one kind occupational configuration of 108-atom supercell was used, whereas in our current calculations we have considered all possible 24 occupational configurations of 20-atom SQS unit cell for the average. Notably, it can be seen a significant difference between the averaged local magnetic moments of the FeCrCoNi HEA with and without vacancy. The system without any vacancy has a lower averaged local magnetic moment than the system with vacancy. Also, it has a lowest total averaged local magnetic moment of 0.270 μ_B/atom. When a vacancy is formed in the FeCrCoNi HEA, the total averaged local magnetic moment μ varies from 0.284 μ_B/atom to 0.414 μ_B/atom, and the largest one occurs in the systems containing a Fe vacancy. In all cases, Ni vacancy has the least effect on averaged local magnetic moments, and the values are closer to the case of the structures without any vacancy. The results show that the main change occurs in the amplitude of the averaged local magnetic moments caused by Fe, Cr and Co vacancy. For a single element, the averaged local magnetic moment of Fe is most affected by Fe vacancy, which increases from 0.576 μ_B/atom to 1.0 μ_B/atom, followed by Cr vacancy. Cr vacancy shows the most significant influence on the averaged local magnetic moment of Ni, Cr and Co, and the absolute value higher by about 0.076 μ_B/atom, 0.204 μ_B/atom and 0.330 μ_B/atom than the cases without vacancy, and the next is the Fe vacancy. Compared with Fe and Cr vacancies, the Co vacancy has little effect on the averaged local magnetic moment.

Furthermore, three-dimensional visualization of the nearest neighboring distances and their local moments of Fe-Cr, Fe-Co, Fe-Fe and Fe-Ni for the FeCrCoNi HEA with and without vacancies, are shown in Fig. 5. Whether the system has vacancies or not, Fe-Ni has the largest averaged nearest neighboring distance. The second largest averaged nearest neighboring distance is the Fe-Co. The smallest is Fe-Cr, which has roughly the same distance as that of Fe-Fe. Overall, the averaged nearest neighboring distances between Fe-*X* (Cr, Co, Fe and Ni) are basically maintained among 2.46–2.50 Å. In compare with the systems without any vacancy, the vacancy formed in the FeCrCoNi HEA generally causes a significant fluctuation in the nearest neighboring distances. As shown in Fig. 5, Fe atoms are mostly ferromagnetically aligned with respect to Cr, Co and Fe atoms sitting in the first nearest neighbor shell of Fe. When Ni atoms sit in the first nearest neighbor shell of Fe atoms, the magnetic moments of Fe atoms are uniformly distributed among positive and negative values. Although magnetic performance of HEAs attracts great attention and their magnetic moments can be sensitive to the base alloy, the addition of alloying elements, and the resulting phase crystal structures [81–83]. From these findings, it can be clearly outlined that the local magnetic moment is also sen-

sitive to the vacancy and their interaction, which will be another factors to be considered to design magnetic HEAs.

5. Conclusions

In difference from traditional metallic materials, such as steels and superalloys, HEAs highlight multicomponent, random and solute alloys, thereby resulting in various different local and, sometimes, severe distorted environments. Within this situation, the same type of constituents in HEAs will have very different thermodynamic quantities of point defects. In this work, we have proposed a computational method to derive defect formation enthalpies for HEAs using the first-principles calculations within the framework of Density Functional Theory in combination with the small-unit-cell SQS structures. The advantages of this method consider all possible configuration and local environments with the established SQS cell. Using the four-component equiatomic HEA alloy of the FeCoCrNi composition as a benchmark example, we have established 24 different occupational configurations on basis of the 20-atom ordered SQS structures. To derive vacancy formation enthalpies of Fe, Co, Cr, and Ni, in totally we have performed the DFT optimized calculations of 480 configurations containing monovacancy.

Using the example of the FeCoCrNi HEA, we first derived its enthalpy of formation for all 24 SQS configurations considered. The obtained enthalpies of formation are all positive, implying that this FeCoCrNi HEA would be metastable. Upon different local occupational configurations, the discrepancies of the enthalpies of formation are highly varied. In average, we obtained the enthalpy of formation of 84.4 meV/atom, in reasonable agreement with the previously reported data of 77 meV/atom for which only one SQS configuration was considered. The derived vacancy formation enthalpies for each component in HEAs vary in a relatively wide range. Upon different local coordinates, the vacancy formation enthalpy is from 0.72 eV to 2.89 eV for Fe, 0.88 eV to 2.90 eV for Co, 0.78 eV to 3.09 eV for Cr, and 0.91 eV to 2.95 eV for Ni. In average, the vacancy formation of enthalpies is 1.58 eV, 1.61 eV, 1.70 eV and 1.89 eV for Fe, Cr, Co and Ni, respectively. Statistically, the vacancies of both Ni and Co should be a bit difficult to be created than both Fe and Cr. The average vacancy formation enthalpies of 1.58 eV for Fe, 1.61 eV for Cr, 1.70 eV for Co and 1.89 eV for Ni are all larger than that (1.41 eV) of pure nickel. This fact seems to imply that the vacancies are much more difficult to be created than in nickel, indicating a reasonable agreement with the recent experimental observation that the FeCoCrNi HEA exhibits two orders of amplitudes enhancement of radiation tolerance with the suppression of void formation at elevated temperatures than in pure nickel. It has been found that the vacancy shows a significant impact for the local spin magnetic moment around the vacancies. Through the analysis of local magnetic moments, the main change occurs in the amplitude of the averaged local magnetic moments caused by Fe, Cr and Co monovacancy, while Ni vacancy has the least effect on averaged local magnetic moments.

Acknowledgements

This work was supported by the National Science Fund for Distinguished Young Scholars (No. 51725103), by the National Natural Science Foundation of China (Grant Nos. 51671193 and 51474202), and by the Science Challenging (Project No. TZ2016004), as well as by the "Hundred Talented Project" of the Chinese Academy of Sciences. Xiongjun Liu and Z. P. Lu at USTB are financially supported by the National Natural Science Foundation of China (Nos. 51671018 and 51671021), 111 Project (No. B07003), International S&T Cooperation Program of China (No. 2015DFG52600), the Program for Changjiang Scholars and Innovative Research Team in University of China (No. IRT_14R05) and the Projects of SKL-AMM-USTB (Nos. 2016Z-04, 2016-09 and 2016Z-16). C. T. Liu at CityU is supported by the Hong Kong URC grant under the contract with City University of Hong Kong. All calculations have been performed on the high-performance computational cluster in the Shenyang National University Science and Technology Park and the National Supercomputing Center in Guangzhou (TH-2 system).

References

[1] A. Glensk, B. Grabowski, T. Hickel, J. Neugebauer, Phys. Rev. X 4 (2014) 011018.
[2] W.W. Xing, P.T. Liu, X.Y. Cheng, H.Y. Niu, H. Ma, D.Z. Li, Y.Y. Li, X.-Q. Chen, Phys. Rev. B 90 (2014) 144105.
[3] B. McKee, W. Triftshäuser, A. Stewart, Phys. Rev. Lett. 28 (1972) 358–360.
[4] G. Neumann, V. Tölle, C. Tuijn, Physica B 271 (1999) 21–27.
[5] P.T. Liu, S.L. Wang, D.Z. Li, Y.Y. Li, X.-Q. Chen, J. Mater. Sci. Technol. 32 (2016) 121–128.
[6] H. Ma, X.Q. Chen, R.H. Li, S.L. Wang, J.H. Dong, W. Ke, Acta Mater. 130 (2017) 137–146.
[7] B. Meyer, M. Faehnle, Phys. Rev. B 59 (1999) 6072.
[8] M. Krcmar, C.L. Fu, A. Janotti, R.C. Reed, Acta Mater. 53 (2005) 2369–2376.
[9] S.L. Shang, B.C. Zhou, W.Y. Yang, A.J. Ross, X.L. Liu, Y.J. Hu, H.Z. Fang, Y. Wang, Z.K. Liu, Acta Mater. 109 (2016) 128–141.
[10] W.W. Xing, X.-Q. Chen, P.T. Liu, X. Wang, P.C. Zhang, D.Z. Li, Y.Y. Li, Int. J. Hydrog. Energy 39 (2014) 18506–18519.
[11] Y.F. Ye, Q. Wang, J. Lu, C.T. Liu, Y. Yang, Mater. Today 19 (2016) 349–362.
[12] J.W. Yeh, S.K. Chen, S.J. Lin, J.Y. Gan, T.S. Chin, T.T. Shun, C.H. Tsau, S.Y. Chang, Adv. Eng. Mater. 6 (2004) 299–304.
[13] B. Cantor, I.T.H. Chang, P. Knight, A.J.B. Vincent, Mater. Sci. Eng. A 375–377 (2004) 213–218.
[14] C.Y. Hsu, J.W. Yeh, S.K. Chen, T.T. Shun, Metall. Mater. Trans. A 35 (2004) 1465–1469.
[15] P.K. Huang, J.W. Yeh, T.T. Shun, S.K. Chen, Adv. Eng. Mater. 6 (2004) 74–78.
[16] Y.Y. Chen, T. Duval, U.D. Hung, J.W. Yeh, H.C. Shih, Corros. Sci. 47 (2005) 2257–2279.
[17] Y.J. Hsu, W.C. Chiang, J.K. Wu, Mater. Chem. Phys. 92 (2005) 112–117.
[18] C.J. Tong, M.R. Chen, S.K. Chen, J.W. Yeh, T.T. Shun, S.J. Lin, S.Y. Chang, Metll. Mater. Trans. A 36 (2005) 1263–1271.
[19] C.J. Tong, M.R. Chen, S.K. Chen, J.W. Yeh, T.T. Shun, S.J. Lin, S.Y. Chang, Metll. Mater. Trans. A 36 (2005) 881–893.
[20] X.F. Wang, Y. Zhang, Y. Qiao, G.L. Chen, Intermetallics 15 (2007) 357–362.
[21] Y.J. Zhou, Y. Zhang, Y.L. Wang, G.L. Chen, Mater. Sci. Eng. A 454–455 (2007) 260–265.
[22] Y.J. Zhou, Y. Zhang, Y.L. Wang, G.L. Chen, Appl. Phys. Lett. 90 (2007) 181904.
[23] U.S. Hsu, U.D. Hung, Y.W. Yeh, S.K. Chen, Y.S. Huang, C.C. Yang, Mater. Sci. Eng. A 460–461 (2007) 403–408.
[24] Y.J. Zhou, Y. Zhang, T.N. Kim, G.L. Chen, Mater. Lett. 62 (2008) 2673–2676.
[25] F.J. Wang, Y. Zhang, Mater. Sci. Eng. A 496 (2008) 214–216.
[26] Y. Zhang, Y.J. Zhou, X.D. Hui, M.L. Wang, G.L. Guo, Sci. China Ser. G 51 (2008) 427–437.
[27] C.Z. Yao, P. Zhang, M. Liu, G.R. Li, J.Q. Ye, P. Liu, Y.X. Tong, Electrochim. Acta 53 (2008) 8359–8365.
[28] Y.J. Zhou, Y. Zhang, F.J. Wang, Y.L. Wang, G.L. Chen, J. Alloys Compd. 466 (2008) 201–204.
[29] Y.P. Wang, B.S. Li, M.X. Ren, C. Yang, H.Z. Fu, Mater. Sci. Eng. A 491 (2008) 154–158.
[30] Y.J. Zhou, Y. Zhang, F.J. Wang, G.L. Chen, Appl. Phys. Lett. 92 (2008) 241917.
[31] C. Li, M. Zhao, J.C. Li, Q. Jiang, J. Appl. Phys. 104 (2008) 113504.
[32] Y. Zhang, Y.Y. Zhou, J.P. Lin, G.L. Chen, P.K. Liaw, Adv. Eng. Mater. 10 (2008) 534–538.
[33] M.S. Lucas, G.B. Wilks, L. Mauger, J.A. Muñoz, O.N. Senkov, E. Michel, J. Horwath, S.L. Semiatin, M.B. Stone, D.L. Abernathy, E. Karapetrova, Appl. Phys. Lett. 100 (2012) 251907.
[34] K.Y. Tsai, M.H. Tsai, J.W. Yeh, Acta Mater. 61 (2013) 4887–48970.
[35] F. Otto, Y. Yang, H. Bei, E.P. George, Acta Mater. 61 (2013) 2628–2638.
[36] P.P. Bhattacharjee, G.D. Sathiaraj, M. Zaida, J.R. Gatti, C. Lee, C.W. Tsai, J.W. Yeh, J. Alloys Compd. 587 (2014) 544–552.
[37] M.J. Yao, K.G. Pradeep, C.C. Tasan, D. Raabe, Scr. Mater. 72–73 (2014) 5–8.
[38] G.A. Salishchev, M.A. Tikhonovsky, D.G. Shaysultanov, N.D. Stepanov, A.V. Kuznetsov, I.V. Kolodiy, A.S. Tortika, O.N. Senkov, J. Alloys Compd. 591 (2014) 11–21.
[39] Y. Zhang, T.T. Zuo, Z. Tang, M.C. Gao, K.A. Dahmen, P.K. Liaw, Z.P. Lu, Prog. Mater. Sci. 61 (2014) 1–93.
[40] M.H. Tsai, J.W. Yeh, Mater. Res. Lett. 2 (2014) 107–123.
[41] Y. Brif, M. Thomas, I. Todd, Scr. Mater. 99 (2015) 93–96.
[42] I. Toda-Caraballo, P.E.J. Rivera-Díaz-del-Castillo, Acta Mater. 85 (2015) 14–23.
[43] C.Y. Lu, L.L. Niu, N.J. Chen, K. Jin, T.N. Yang, P.Y. Xiu, Y.W. Hang, F. Gao, H.B. Bei, S. Shi, M.R. He, I.M. Robertson, W.J. Weber, L.M. Wang, Nat. Commun. 7 (2016) 1–7.
[44] F. Granberg, K. Nordlund, M.W. Ullah, K. Jin, C.Y. Lu, H.B. Bei, L.M. Wang, F. Djurabekova, W.J. Weber, Y. Zhang, Phys. Rev. Lett. 116 (2016) 135504.

[45] N.A.P.K. Kumar, C. Li, K.J. Leonard, H. Bei, S.J. Zinkle, Acta Mater. 113 (2016) 230–244.
[46] M. Vaidya, S. Trubel, B.S. Murty, G. Wilde, S.V. Divinski, J. Alloys Compd. 688 (2016) 994–1001.
[47] B. Cai, B. Liu, S. Kabra, Y.Q. Wang, K. Yan, P.D. Lee, Y. Liu, Acta Mater. 127 (2017) 471–480.
[48] M.R. He, S. Wang, S. Shi, K. Jin, H.B. Bei, K. Yasuda, S. Matsumura, K. Higashida, I.M. Robertson, Acta Mater. 126 (2017) 182–193.
[49] S.J. Zhao, Y. Osetsky, Y.W. Zhang, Acta Mater. 128 (2017) 391–399.
[50] Y. Yu, J. Wang, J.S. Li, J. Yang, H.C. Kou, W.M. Liu, J. Mater. Sci. Technol. 32 (2016) 470–476.
[51] L. Jiang, Y.P. Lu, W. Wu, Z.Q. Cao, T.J. Li, J. Mater. Sci. Technol. 32 (2016) 245–250.
[52] L. Jiang, H. Jiang, Y.P. Lu, T.M. Wang, Z.Q. Cao, T.J. Li, J. Mater. Sci. Technol. 31 (2015) 397–402.
[53] C. Zhang, F. Zhang, S.L. Chen, W.S. Cao, JOM 64 (2012) 839–845.
[54] M.C. Gao, D.E. Alman, Entropy 15 (2013) 4504–45019.
[55] A.J. Zaddach, C. Niu, C.C. Koch, D.L. Irving, JOM 65 (2013) 1780–1789.
[56] F. Körmann, A.V. Ruban, M.H.F. Sluiter, Mater. Res. Lett. 5 (2017) 35–40.
[57] A. Tamm, A. Aabloo, M. Klintenberg, M. Stocks, A. Caro, Acta Mater. 99 (2015) 307–312.
[58] C. Niu, A.J. Zaddach, A.A. Oni, X. Sang, J.W. Hurt III, J.M. LeBeau, C.C. Koch, D.L. Irving, Appl. Phys. Lett. 106 (2015) 161906.
[59] D. Maa, B. Grabowski, F. Körmannb, J. Neugebauer, D. Raabe, Acta Mater. 100 (2015) 90–97.
[60] Y.W. Zhang, G.M. Stocks, K. Jin, C.Y. Lu, H.B. Bei, B.C. Sales, L.M. Wang, L.K. Béland, R.E. Stoller, G.D. Samolyuk, M. Caro, A. Caro, W.J. Weber, Nat. Commun. 6 (2015) 1–9.
[61] C. Jiang, B.P. Uberuaga, Phys. Rev. Lett. 116 (2016) 105501.
[62] D.J.M. King, S.C. Middleburgh, A.G. McGregor, M.B. Cortie, Acta Mater. 104 (2016) 172–179.
[63] C. Niu, A.J. Zaddach, C.C. Koch, D.L. Irving, J. Alloys Compd. 672 (2016) 510–520.
[64] M.C. Troparevsky, J.R. Morris, P.R.C. Kent, A.R. Lupini, G.M. Stocks, Phys. Rev. X 5 (2015) 011041.
[65] S. Huang, W. Li, X.Q. Li, S. Schönecker, L. Bergqvist, E. Holmström, L.K. Varga, L. Vitos, Mater. Des. 103 (2016) 71–74.
[66] S.J. Zhao, G.M. Stocks, Y.W. Zhang, Phys. Chem. Chem. Phys. 18 (2016) 24043.
[67] S.C. Middleburgh, D.M. King, G.R. Lumpkin, M. Cortie, L. Edwards, J. Alloys Compd. 599 (2014) 179–182.
[68] A. Zunger, S.H. Wei, L.G. Ferreira, J.E. Bernard, Phys. Rev. Lett. 65 (1990) 353.
[69] M.Y. Lavrentiev, J.S. Wróbel, D. Nguyen-Manh, S.L. Dudarev, Phys. Chem. Chem. Phys. 16 (2014) 16049.
[70] J.S. Wróbel, D. Nguyen-Manh, M.Y. Lavrentiev, M. Muzyk, S.L. Dudarev, Phys. Rev. B 91 (2015) 024108.
[71] G. Kresse, J. Furthmüller, Comput. Mater. Sci. 6 (1996) 15–50.
[72] G. Kresse, J. Furthmüller, Phys. Rev. B 54 (1996) 11169–11186.
[73] P.E. Blöchl, Phys. Rev. B 50 (1994) 17953–17979.
[74] G. Kresse, D. Joubert, Phys. Rev. B 59 (1999) 1758–1775.
[75] J.P. Perdew, K. Burke, M. Ernzerhof, Phys. Rev. Lett. 77 (1996) 3865–3868.
[76] A.V.D. Walle, M. Asta, G. Ceder, Calphad 26 (2002) 539–553.
[77] A.V.D. Walle, P. Tiwary, M.D. Jong, D.L. Olmsted, M. Asta, A. Dick, D. Shin, Y. Wang, L.Q. Chen, Z.K. Liu, Calphad 42 (2013) 13–18.
[78] F.R.D. Boer, R. Boom, W.C.M. Mattens, A.R. Miedema, A.K. Niessen, Cohesion in Metals – Transition Metal Alloys, North-Holland, 1988.
[79] X.-Q. Chen, R. Podloucky, Calphad 30 (2006) 266–269.
[80] P. Ehrhart, P. Jung, H. Schultz, H. Ullmaier, Atomic Defects in Metals, In: Landolt-Börnstein, New Series, Group III, vol. 25, Springer-Verlag, Berlin, 1991.
[81] T.T. Zuo, M.C. Gao, L. Ouyang, X. Yang, Y.Q. Cheng, R. Feng, S.Y. Chen, P.K. Liaw, J.A. Hawk, Y. Zhang, Acta Mater. 130 (2017) 10–18.
[82] M.S. Lucas, L. Mauger, J.A. Munoz, Y.M. Xiao, A.O. Sheets, S.L. Semiatin, J. Horwath, Z. Turgut, J. Appl. Phys. 109 (2011) 3.
[83] T.T. Zuo, R.B. Li, X.J. Ren, Y. Zhang, J. Magn. Magn. Mater. 371 (2014) 60–68.